Toughening of Cubic Silsesquioxane Epoxy Nanocomposites Using Core−Shell Rubber Particles: A Three-Component Hybrid System

Jiwon Choi,[‡] Albert F. Yee,[§] and Richard M. Laine*[,†,‡]

Department of Materials Science and Engineering and the Macromolecular Science and Engineering Center, University of Michigan, Ann Arbor, Michigan 48109-2136, and Institute of Materials Research & Engineering, 3, Research Link, Singapore 117602

Received July 7, 2003

ABSTRACT: This study explores the concept of composite construction simultaneously at nano- and macroscopic length scales. This approach promises to allow improvement of multiple properties coincidentally but independently. A model system was identified that allows us to test this concept by combining molecular level hybridization using a silsesquioxane epoxy nanocomposite with macroscopic modification using core−shell rubber particles (CSR). The objective here was to form an epoxy resin system with enhanced thermal stability, elastic modulus, and fracture toughness. The nanocomposite was made by reacting octa(dimethylsiloxyethylcyclohexyl epoxide)silsesquioxane (OC, 1.3 nm diameter) with diaminodiphenylmethane (DDM). This resin offers excellent elastic moduli and thermal stabilities at the expense of poor fracture toughness. OC/DDM is a "single phase" hybrid nanocomposite that is used here as a matrix for ≈100 nm diameter CSR reinforcing particles. Characterization of OC/DDM/CSR composites shows that fracture toughness improves significantly on inclusion of CSR particles with little effect on elastic moduli and thermal stability. Stress and strain at failure also improve, indicating better fracture toughness. SEM studies suggest that shear yielding and CSR pull-out are the likely sources of toughening.

Introduction

Organic/inorganic hybrid nanocomposites offer great potential for novel properties because distinct organic and inorganic component properties can be combined in a single material with uniformity of mixing at the nanoscale. Furthermore, synergistic improvements in properties are often made when the component sizes approach this length scale.[1−15] While early research in hybrid systems focused on the development of polymer-layered silicate nanocomposites,[7−15] one recent trend is to synthesize well-defined hybrid nanobuilding blocks with custom-designed organic functionality and to process nanocomposites from them.[16−18] Motivation for the nanobuilding block approach arises from the knowledge that control of structures/interactions at the smallest scales and the systematic nanometer by nanometer construction of composites provide the best chance to enhance/control macroscopic properties. However, this approach requires an understanding of the nanoscale structure−processing−property relationships of nanocomposites to select the right nanocomponents and to process them properly for the target properties.

To better understand such relationships, we recently initiated studies using cubic silsesquioxanes (cubes, typically 1.2−1.5 nm diameters) to produce completely discontinuous nanocomposites (per Scheme 1).[19−25] In our approach, various functional groups are appended to cubes and then cross-linked to form nanocomposites.

These systems can serve as models for studying various nanostructure relationships because manipulation of the functional groups and the cross-linking chemistry provides excellent control of nanoscale construction parameters, especially organic tether structure, architecture, rigidity, cross-link density, etc. Changes in properties associated with changes in these parameters can be followed by various analytical tools.[19−21]

In the course of these studies, features common to all silsesquioxane nanocomposites were identified. First, these nanocomposites are homogeneous, and no phase segregation occurs even at the 1−2 nm length scale. Second, organic tether structures determine the nanocomposite mechanical properties. Last, manipulation of tether structure can radically change nanocomposite thermal behavior. In other words, tether design is the limiting factor as well as the guideline for modifying nanocomposite properties by manipulation at nanometer length scales.

These findings provided the impetus to explore nanocomposite modification at macroscopic scales in the hope that (1) properties that are not effectively controlled at one length scale can be better controlled at another and (2), more importantly, to prove that multiple properties can be independently modified at two different length scales.

In practice, cube "single phase" hybrid nanocomposites can be used as matrices for macroscopic composites because of their extreme homogeneity. Then, numerous macroscopic composite methodologies can be adopted to further modify hybrid matrix properties. That is, on the nanoscale, we have the opportunity to tailor the matrix by selecting cube tethers with specific organic architectures that define basic thermomechanical properties. On the macroscale, we can then add reinforcements based on traditional composite approaches to selectively improve target properties.

The ideal model system for this approach would possess at least one property that can be modified by traditional methods. Usually, it is difficult to optimize

[†] Department of Materials Science and Engineering, University of Michigan.
[‡] Macromolecular Science and Engineering Center, University of Michigan.
[§] Institute of Materials Research & Engineering.
* Address correspondence to this author.

10.1021/ma0303723 CCC: $27.50
Published on Web 04/08/2004

Scheme 1. Formation of the Nanocomposites (II) from Cubic Silsesquioxane (I)

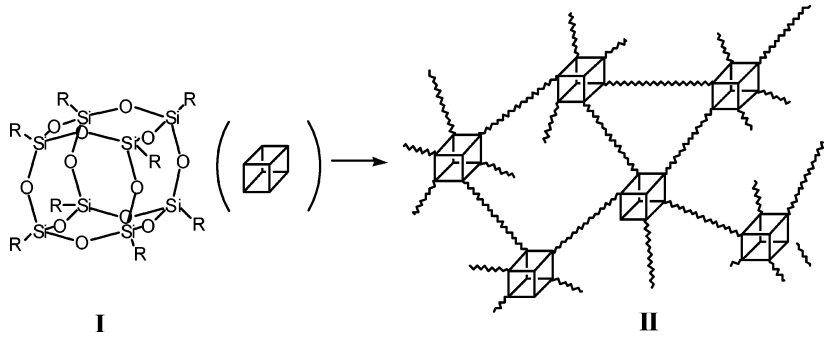

I II

all of the properties at once in developing new composites. Sometimes, improving some properties results in degradation of others. For example, polymer composites with well-dispersed layered silicates often offer improved thermal stability and elastic modulus, but at the expense of fracture toughness.[14−16] A similar trend was observed in epoxy cube nanocomposite studies.[21] Increasing tether rigidity improves thermal stability and elastic modulus but decreases the fracture toughness. Given these results, an epoxy cube nanocomposite with good elastic modulus and poor fracture toughness can serve as a model system where fracture toughness can be improved by traditional toughening strategies as an example of macroscale modification. Furthermore, organic epoxy resins are widely studied as matrices for composites filled with nanosized inorganic reinforcements such as silica particles[26−28] or layered silicates,[29−33] offering good reference for comparison.

In modifying nanocomposites by traditional approaches, it is desired that properties improve independently. In other words, inherent nanocomposite properties should not be degraded as a result of macroscale modification or the changes should be minimal. If correct, this model study could provide a new strategy for modifying multiple properties independently in a single composite.

Here, we demonstrate the concept of combining molecular level hybridization with macroscopic modification of composite properties using an epoxy cube nanocomposite matrix.[19−21] The selection of the specific epoxy cube nanocomposite is first justified. Then, the basic properties of the epoxy cube nanocomposite are used to determine the toughening strategy. Thereafter, various properties are measured to evaluate the effectiveness of this new approach.

Experimental Section

Materials. Diaminodiphenylmethane (DDM) was purchased from Alfa Aesar (Ward Hill, MA) and used without further purification. An aqueous suspension of core shell rubber (CSR, ∼40 wt % in suspension) particles was provided by Professor H.-J. Sue of Texas A&M University.[34,35] Octa-(dimethylsiloxyethylcyclohexenyl epoxide)silsesquioxane (OC) was synthesized following literature procedures.[21]

Processing. *OC/DDM Curing.* In formulating OC/DDM nanocomposites, a variable N was defined as discussed in previous papers.[21,22] Thus, when $N = 1$, there are equal numbers of NH_2 groups and epoxy rings in the sample mixture. In practice, for the formulation of $N = 1.0$, 3.40 g (17.17 mmol) of DDM and 8.60 g (4.28 mmol) of OC (total 12 g) were used to prepare composites.

Materials were weighed into an aluminum pan (61.5 mm diameter × 18 mm) and mixed by hand. The mixture was melted and degassed at 140−150 °C under vacuum for 7−15 min. When the mixture became homogeneous and no more bubbles emerged, it was poured into an aluminum mold previously surface-coated with Teflon mold release agent and preheated to 150 °C. The mixture was then cured at various temperatures under nitrogen for various periods of time. After the mold cooled, the sample was removed, rough edges were polished on a polish wheel with 180, 600, and 1200 grit SiC paper, and the sample was kept in a desiccator prior to testing.

Table 1. Formulation of OC/DDM/CSR Nanocomposites

CSR loading	0.0 wt %	4.0 wt %	8.0 wt %
OC/CSR (g) (mmol of OC)[a]	0	0.58 (0.23)	1.18 (0.47)
(CSR, g)[b]	(0)	(0.12)	(0.24)
g of neat OC (mmol)	2.87 (1.43)	2.32 (1.15)	1.76 (0.87)
g of DDM (g) (mmol)	1.13 (5.72)	1.10 (5.56)	1.06 (5.35)

[a] mmol of OC in OC/CSR: 80 wt % of OC/DDM mass is assumed as the net mass of OC. [b] CSR mass: 20 wt % of OC/CSR mass.

Core−Shell Rubber (CSR) Particles. CSR particles used in the study are styrene−butadiene copolymers. Their properties and processing have been described in previous publications.[34,35] CSR diameters are ≈100 nm based on preliminary SEM/TEM studies.[36] First, 50 mL of an aqueous suspension of CSR particles was mixed with 100 mL of methyl ethyl ketone (MEK) and 50 mL of deionized water in a 500 mL beaker. The solution was then transferred to a separatory funnel and let stand for 1 h. When the solution separated into two layers, the aqueous layer was removed. The funnel was rinsed with a small amount of MEK, and another 50 mL of deionized water was added. The solution was well shaken and then left idle for another 20 min followed by separation of the aqueous layer. The extraction/separation step was repeated five times. Finally, about 100 mL of organic layer (CSR/MEK solution) was collected and used immediately for preparing nanocomposites.

OC/DDM/CSR Nanocomposites. OC monomer (50 g, 24.86 mmol) was first dissolved completely in 50 mL of CSR/MEK solution, and then the solution was vacuum-dried to give a solid OC/CSR mixture. The CSR content in the OC/CSR mixture was determined by comparing the mass of the sample solution before (2.5 g of neat OC in 5 vol % of the final OC/CSR/MEK solution) and after the solvent was vacuum-dried (a combined mass of 3.1 g of OC and CSR). Thus, the weight fraction of CSR in the OC/CSR mixture was estimated to be ∼20 wt %.

Melt Processing. Nanocomposites with three CSR loadings were prepared. Table 1 summarizes the formulations of 0.0, 4.0, and 8.0 ± 0.1 wt % CSR loaded nanocomposites. Neat OC and DDM (total 4.00 g) were weighed separately, introduced into an aluminum pan (61.5 mm diameter × 18 mm), and melted together at 200 °C. The resulting melt was first stirred by hand, then degassed under vacuum for 5−7 min, and transferred into an aluminum mold (30 × 13 × 30 mm). Samples were then cured under N_2 at 200 °C for 24 h. The prepared nanocomposite was characterized by optical microscopy to identify/assess phase segregation.

Solution Processing. Formulations in Table 1 were prepared using this process. The OC/CSR mixture, neat OC, and DDM (total 4.00 g) were separately weighed and dissolved together

Scheme 2. Preparation of Optical Microscope (OM) Image Samples: (a) OM Sample with Full Indentation; (b) OM Sample with Halved Indentation via Microtoming

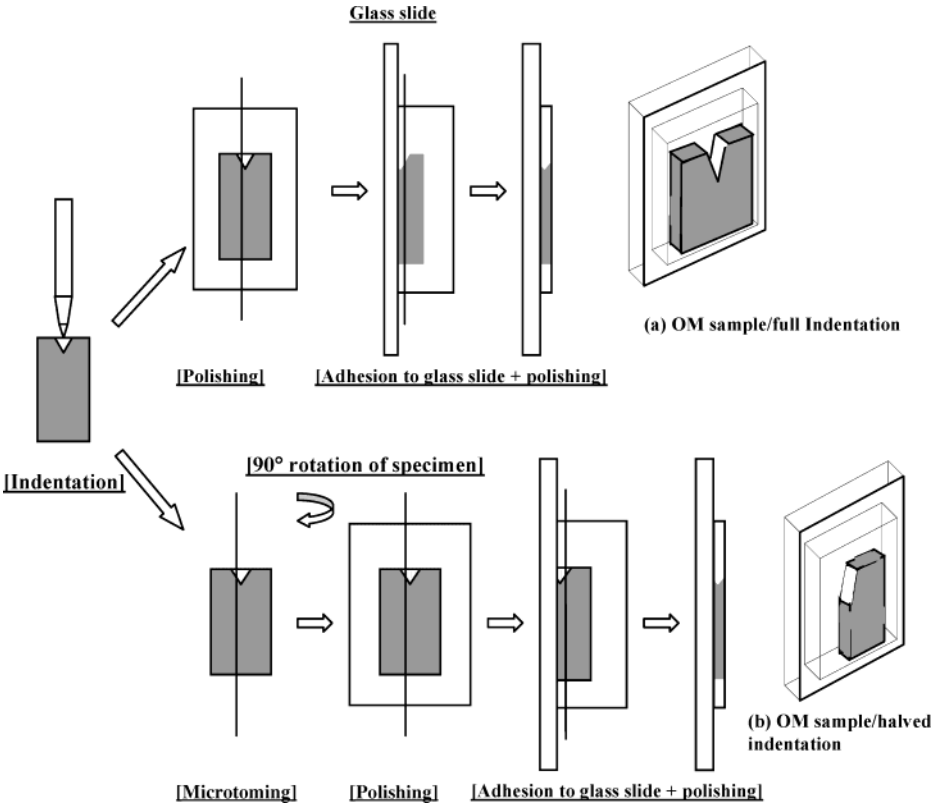

in 10 mL of MEK in a 20 mL vial. The solution was then transferred to an aluminum pan (61.5 mm diameter × 18 mm). MEK was removed under vacuum at 200 °C for 5−7 min, and the resulting melt was poured into an aluminum mold (30 × 13 × 30 mm) and cured under N_2 at 200 °C for 24 h. The prepared nanocomposites were initially examined for phase segregation by optical microscopy and then further characterized using DMA and TGA.

Fracture toughness specimens were prepared using the same procedure but in a 9 × 5 × 40 mm aluminum mold. For the preparation of tensile and compression test specimens, a dog bone-shaped mold (2 mm neck thickness × 3.2 mm neck width × 60 mm length) and a cylindrical mold (9.5 diameter × 19 mm length) were used.

Characterization. To assess the toughenability of these rather brittle materials, indentation studies were performed using a Teledyne-Table shear/scratch tester model 502. Indentations were made on the surfaces of neat OC/DDM nanocomposites using a diamond stylus (90° angle, 76 μm radius). An arbitrary force was applied by hand. The prepared specimens were embedded in epoxy resin and cured for 24 h. Samples were then carefully polished using 600, 1200, and 400 grit SiC papers and 5, 1, 0.3, and 0.05 μm alumina powder suspensions until the center of the indentation was exposed. The polished surface was glued to a glass slide using epoxy resin and cured at room temperature for 24 h. The remaining sections were then polished into ~50 μm thick specimens. The prepared specimens were kept in a desiccator until characterization by optical microscopy (OM).

To prepare samples for assessing the amount of residual elastic stress caused by the indentation test, the indented samples were cut in half by microtoming. Then, the other sample halves were embedded in epoxy resin and processed into OM specimens as described above. These steps were schematically illustrated in Scheme 2.

All of the OM specimens were studied using an Olympus BH-2 optical microscope. Cross-polarized light was used to view the birefringence with magnifications up to ×1000. The images were recorded using a SONY color video CCD camera, DXC-151A (resolution = 768 × 493 pixels).

Fracture Toughness Testing. The critical stress intensity factor (K_{IC}) was measured in the three-point bending mode following ASTM standard E399 (1990). Specimens were polished to 8.50 (B) × 4.25 (w) × 40.0 mm bars. The span of the two support beams was 30.5 mm. A 0.5 mm notch was made in the sample using a hacksaw, and a natural crack was introduced using a new razor blade. The ratio of the crack to the thickness (B) was 0.35−0.55. The sample was then loaded in an Instron testing machine, and force was applied at a constant crosshead rate of 1 mm/min until the sample broke. The load at fracture was recorded. The critical stress intensity factor was calculated from the following equations:

$$K_{IC} = Y\sigma_0 a^{1/2}$$

$$Y = \left[1.93 - 3.07\left(\frac{a}{w}\right) + 14.53\left(\frac{a}{w}\right)^2 - 25.11\left(\frac{a}{w}\right)^3 + 25.80\left(\frac{a}{w}\right)^4\right]$$

$$\sigma_0 = \frac{3SP_b}{2Bw^2}$$

where P_b is the load at fracture, B is the sample thickness, w is the sample width, S is the span, and a is the crack length.

Thermal Gravimetric Analyses (TGA). Thermal stabilities of materials were tested under nitrogen or air using a model 2960 DTA-TGA Instrument (TA Instruments, Inc., New Castle, DE). Samples (15−25 mg) were loaded in platinum pans and ramped to 1000 °C (5 °C/min/N_2). The N_2 or air flow rate was 60 mL/min.

Dynamic Mechanical Analyses (DMA). Dynamic mechanical behavior of cured samples was studied using a TA instruments 2980 dynamic mechanical analyzer (New Castle, DE). Cured samples were polished to ≈3.0 × 13.0 × 30.0 mm and mounted on a single cantilever clamp. The mechanical properties were measured under nitrogen in step mode in 10 °C intervals from −50 to 200 °C. Prior to each measurement, the environment was kept at the setting temperature for 10 min to ensure thermal equilibration.

Table 2. Selected Properties for Various Epoxy Cube Nanocomposites ($N = 1$);[19−21] Properties of the Organic Epoxy Resin (DGEBA/DDM)[19,20] Are Included for Comparison

nanocomposites	T_d(5%)[e] (° C)	T_d(20%)[f] (° C)	CY[g] (%)	char Y (%)	modulus (GPa)	K_{IC} (MPa m$^{1/2}$)	T_g (° C)
OC/DDM	415	450	31	34	2.3	0.5	110
OG/DDM[a]	344	408	32	40	1.8	1.2	60
OG/OC/DDM[b] ($N = 1.25$)	350	416	31	35	2.3	1.8	60
DGEBA[c]/OAPS[d]	355	384	17.6	43	2.4		*h*
DGEBA/DDM	338	368	0	17	2.4	1.3	110

[a] OG = octa(glycidyldimethylsiloxy)silsesquioxane. [b] OG/OC/DDM = blending of 75 mol % OG/25 mol % OC at $N = 1.25$. [c] DGEBA = diglycidyl ether of bisphenol A. [d] OAPS = octaaminophenylsilsesquioxane. [e] T_d(5%) = 5% mass loss temperature in TGA (N_2/5 °C/min). [f] T_d(20%) = 20% mass loss temperature in TGA (N_2/5 °C/min). [g] CY = ceramic yield at 1000 °C (air/5 °C/min). [h] No T_g.

Scheme 3. Structures of OC and DDM

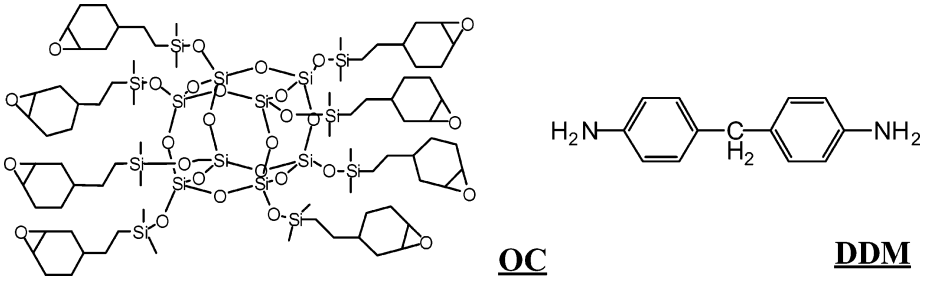

Compression tests were performed using a screw-driven Instron 4502 following ASTM standard E9-89a (2000). Cylindrical samples with a diameter of 9.5 mm and a length of 19 mm were used for the tests. The cross-head speed was set at 1 mm/min. Data were recorded at a rate of 10 points/s. The tests were continued until the samples failed completely.

Tensile testing was also performed using a screw-driven Instron 4502 following ASTM standard E111 (1997). Dog bone samples with a thickness of ∼2 mm and a width of ∼3.2 mm were used for all of the formulations. The cross-head speed was set at 1 mm/min. Data were recorded at a speed of 10 points/s. The tests were continued until the samples failed.

Scanning Electronic Microscopy (SEM). Fractured samples were mounted on a holder and a thin layer (≈5 nm) of Au/Pd was applied on to the fracture surfaces using a Technics Hummer VI sputter coater. SEM images were then taken using a Philips XL 300 FEG SEM at an acceleration voltage of 5 kV under high vacuum.

Results

Demonstration of independent property modification at two length scales requires a composite that already exhibits improved properties as a result of tether manipulation and at least one poor property that can be further improved by macroscopic composite methods with minimum interference with the nanoscale modifications. Table 2 shows selected properties of epoxy tether nanocomposites studied to date.

Comparison of these properties indicates that octa(dimethylsiloxyethylcyclohexylepoxy)silsesquioxane (OC)/diaminodiphenylmethane (DDM) exhibits the best thermal stability and higher elastic modulus than its OG/DDM counterpart, perhaps as a result of tether rigidity, but it also has the poorest fracture toughness. Thus, it may require toughening using the right strategy. Previous studies[19,21] show that improving fracture toughness by tailoring tether structure (OC/DDM vs OG/DDM) results in decreases in modulus and thermal stability. Improving modulus and toughness simultaneously by blending OG and OC also degrades thermal stability and the glass transition temperature.[21] Thus, independent improvement of all these properties only at the nanoscale seems difficult at best; however, the fracture toughness of epoxy resins is often modified by the addition of macroscopic toughening such as rubber, thermoplastic, or inorganic particles.[37−58] We show in this paper that one of these toughening strategies is indeed successful. Given these results, OC/DDM can serve as a model system for property modification at two length scales, where fracture toughness can be modified by macroscopic modification. A practical goal in this study is to develop nanocomposites with enhanced thermal stability, elastic modulus, and fracture toughness.

We begin by reviewing the OC/DDM properties reported previously followed by OC/DDM nanoindentation studies to determine whether the proposed toughening strategy is feasible. Note that the silsesquioxane cube component = hard particle is ≈1.4 nm in diameter. On the basis of these results, core−shell rubber (CSR) particles with sizes 2 orders of magnitude larger (diameters ≥ 100 nm) were chosen as potential toughening.[37−51] Processing conditions were developed to produce homogeneous nanocomposites with improved fracture toughness. Then, properties were assessed by fracture toughness measurements, TGA, DMA, tensile, and compression tests. Last, SEM studies of fractured surfaces were conducted to identify the toughening mechanism(s).

Matrix Characterization. *OC/DDM Nanocomposite Base Properties.* The synthesis and characterization of OC are reported elsewhere[21] and thus are not discussed here. OC is a white solid with a T_m of 125 °C. It is readily amine cured in the melt providing that both components are miscible. In formulating OC/DDM nanocomposites the "variable N" was defined (see Experimental Section) such that when $N = 1$, there are equal numbers of NH_2s and epoxy rings in the sample mixture. A conventional stoichiometric ratio of 2 mol of amine to 1 mol of epoxy would occur for $N = 0.5$.[59−61] Scheme 3 shows the OC and DDM molecular structures.

Our previous studies[19,21] show that the OC/DDM modulus increases to >3 GPa (cured 150 °C/10 h) at $N = 1.5$ as the DDM content increases, while fracture toughness remains at 0.5 ± 0.1 MPa m$^{1/2}$ for all compositions studied. It was also found that the simplest OC/DDM nanonetwork structure was obtained at $N = 1.0$ with the highest glass transition temperature of

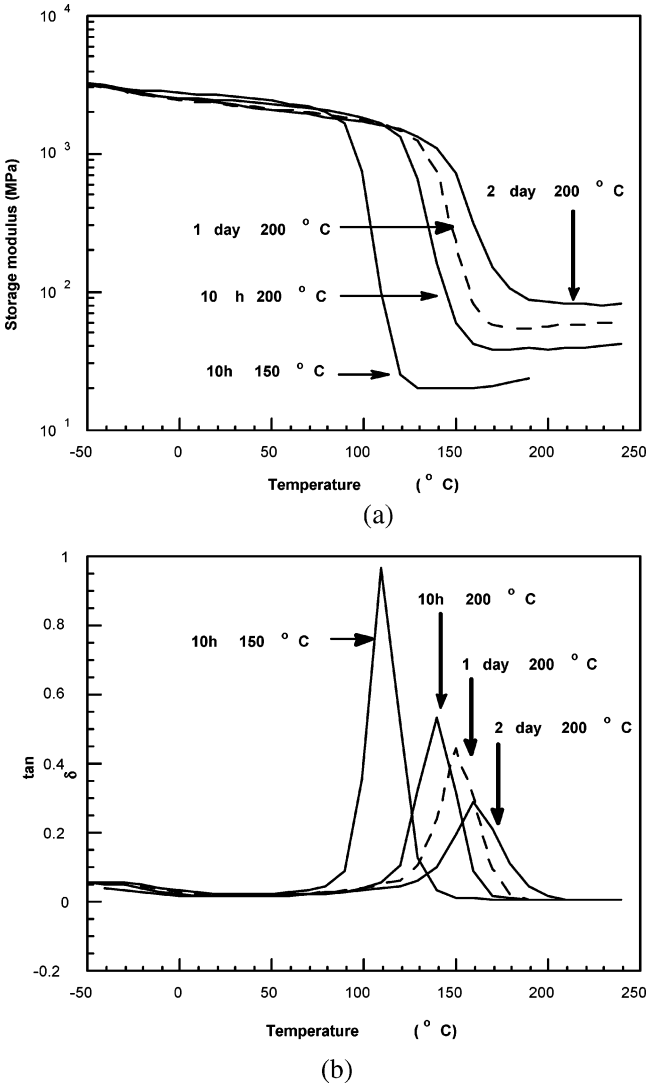

Figure 1. DMA of OC/DDM cured under selected conditions (1 Hz): (a) storage modulus; (b) tan δ.

≈110 °C and 5% mass loss temperature of ≈415 °C (TGA under N_2 at 5 °C/min ramp). Therefore, the formulation $N = 1.0$ was selected as a standard matrix in studies reported here.

Glass Transition Temperature Modification. The base T_g of OC/DDM is only 110 °C after curing at 150 °C/10 h following the method adopted previously. Because a high glass transition temperature (T_g) is essential for composites used for high-temperature applications and matrices with low T_gs can be toughened easily, an attempt was made to maximize T_g by varying the cure temperatures and times. Figure 1 shows OC/DDM DMA results using various curing conditions.

In the DMA profiles, it appears that higher curing temperatures and longer times produce OC/DDM with higher T_gs. The rubbery plateau moduli also increase with increasing T_gs, suggesting increasing cross-link densities. Tan δ profiles permit convenient and precise identification of T_gs. The highest T_g observed is ≈160 °C after a 2 day cure at 200 °C. This result suggests that higher temperatures overcome viscosity/diffusion barriers allowing curing of remaining unreacted end groups (defects), which in turn further increase the cross-link density. However, a 1 day cure at 200 °C provides a $T_g \approx 150$ °C and was adopted as a practical cure cycle.

Nanoindentation Study. In general, the effectiveness of toughening strategies is greatly affected by the matrix's intrinsic plasticity.[53,54,62−64] If the matrix exhibits plasticity, its capacity to absorb fracture energy can improve when soft cavitating materials such as rubber trigger plastic deformation. If the matrix exhibits little plasticity, materials that can absorb fracture energy within themselves such as thermoplastic tougheners are preferred. Therefore, to determine whether OC/DDM nanocomposites deform in plastic shear, surface indentations with a diamond stylus and optical microscopy (OM) were used to characterize deformation behavior.

First, an arbitrary force is applied with a diamond stylus (90° angle, 76 μm radius) to the composite's surface, and cross sections of indentations are viewed by OM under crossed polars (Figure 2a,b).

In these images, significant birefringence is observed around the indentation pit due to matrix deformation. Small cracks beneath the indented surface also cause some birefringence, but only small cracks were observed and only near the indent center. Thus, they contribute little to the birefringence and can be ignored for assessing the extent of plastic deformation. In fact, birefringence is stronger in regions without cracks, indicating significant plastic or trapped elastic deformation.

To differentiate between birefringence caused by plastic deformation from potentially trapped elastic deformation, i.e., residual stress due to the plastic deformation, half the indentation was removed to release the frozen-in stress. Indented cross sections were cut to half by microtoming and examined by OM (Figure 3a,b). (It should be noted that these sections are already quite thin; thus, it is thought that halving the section

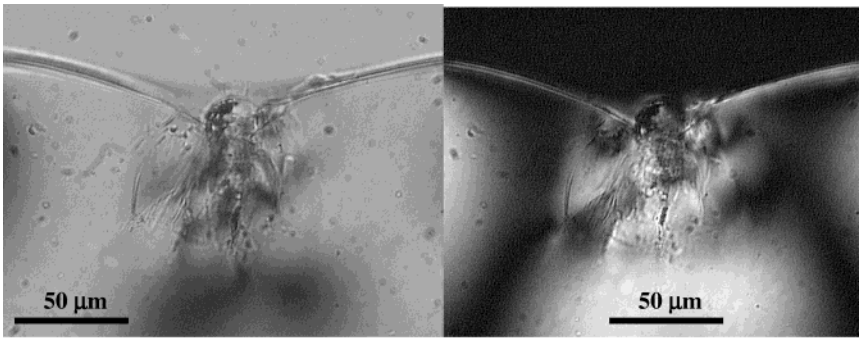

Figure 2. OM images of cross sections of indentations on OC/DDM made by a diamond stylus: (a) unpolarized light; (b) cross-polarized light.

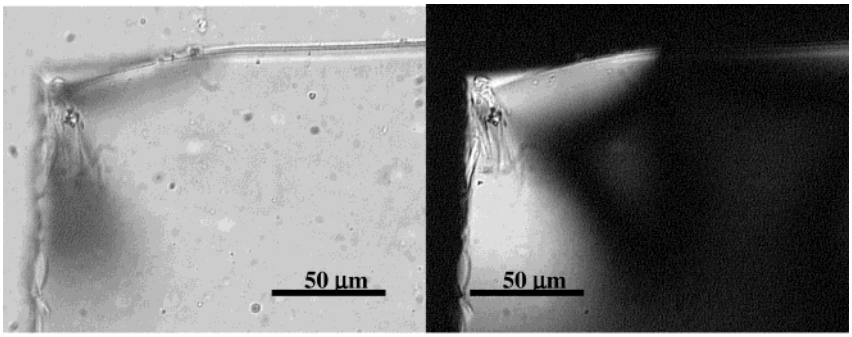

Figure 3. OM images of halved cross sections of indentations on OC/DDM made by a diamond stylus: (a) unpolarized light; (b) cross-polarized light. The bright areas in (b) are due to birefringence.

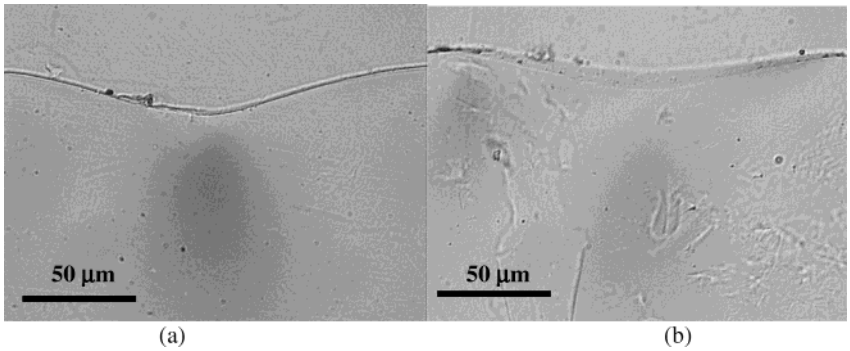

Figure 4. Upolarized OM images of OC/DDM cross sections after CSR incorporation: (a) solution processed; (b) melt processed.

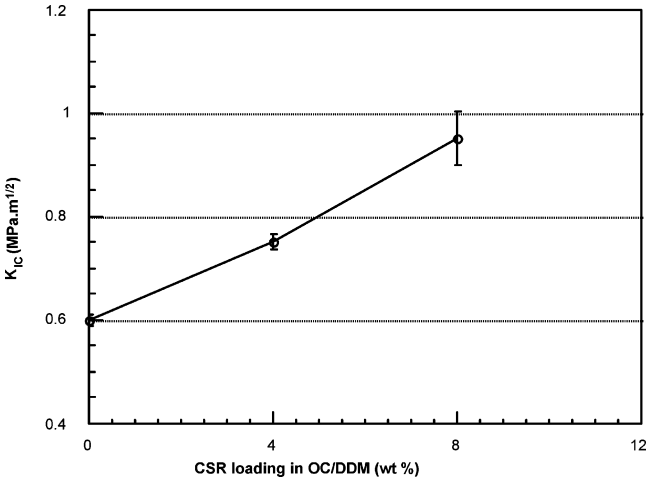

Figure 5. Improvement of OC/DDM fracture toughness vs CSR loading.

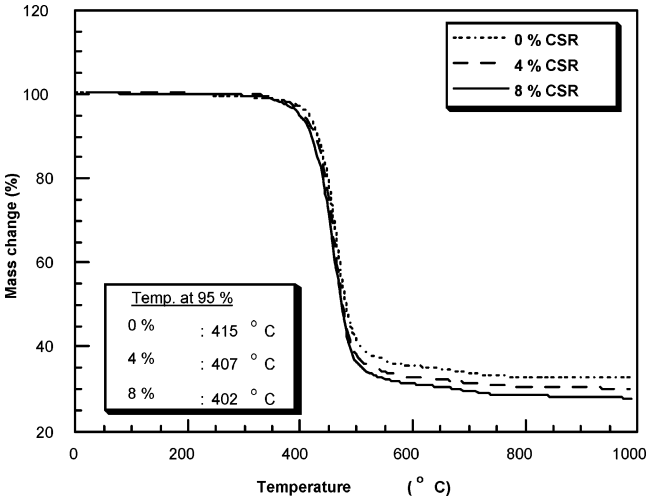

Figure 6. TGA of OC/DDM/CSR nanocomposites (N_2/5 °C/min).

perpendicular to its thickness should release any residual stress that might be contributing to the birefringence.) In these micrographs, birefringence is still significant, indicating significant plastic deformation. Therefore, it is thought that OC/DDM is brittle but capable of deforming plastically. This result suggests the toughening strategy, which is described in the following.

Hybrid Matrix Toughening. *CSR Nanocomposites Processing*. The matrix plasticity found in the indentation study suggests that the capacity of the matrix to absorb fracture energy can be improved by incorporating soft, cavitable materials. Thus, core−shell rubber particles (CSRs)[37,38] were chosen to toughen the system. CSRs with diameters from ≈100 nm to several microns have been used to effectively toughen various polymers.[39−51] In these studies, toughening mechanisms that involve crazing, shear yielding, and/or cavitation have been proposed. For cross-linked polymers, enhanced shear yielding is suggested to be the primary reason for improvements in fracture toughness.[45−51]

CSR particles are commercially available as an aqueous suspension[37,38] and must be extracted using organic solvents. In our process, CSR particles were extracted using methyl ethyl ketone (MEK). OC was then dissolved directly in the CSR/MEK solution, and MEK removed by vacuum during cure to prepare a solid OC/CSR mixture. The CSR concentration in this mixture was determined to be ≈20 wt % (see Experimental Section). In preparing OC/DDM/CSR nanocomposites, the 20% CSR/OC was further diluted with pure OC to give 4 and 8 wt % CSR resins.

Two different curing approaches were taken. The first was to redissolve the OC/DDM/CSR mixture in MEK

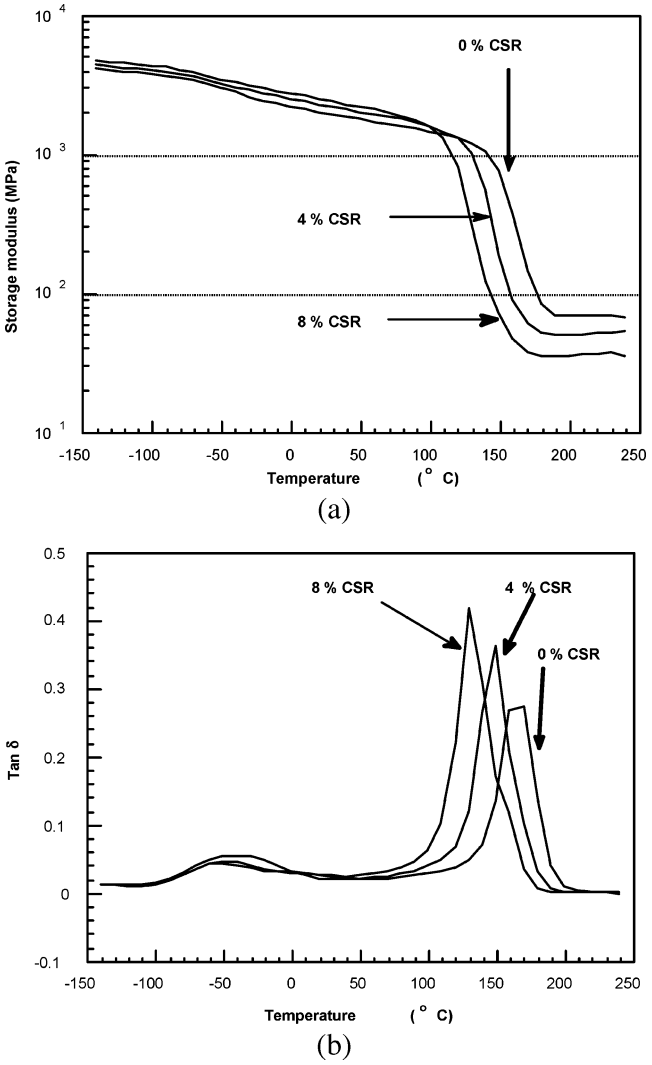

Figure 7. DMA of OC/DDM/CSR nanocomposites (frequency 1 Hz): (a) storage modulus; (b) tan δ.

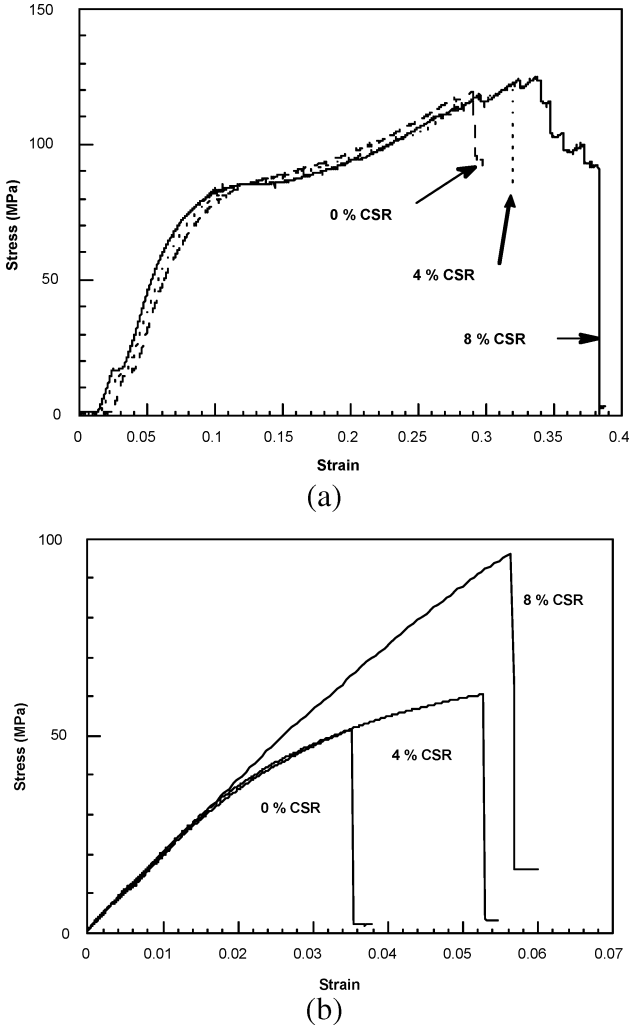

Figure 8. Room temperature mechanical properties tests: (a) compression; (b) tension. Note that the strain scales for (a) and (b) are different.

to form a homogeneous solution and then remove solvent prior to thermal curing (solution process). The second involves melt mixing with simultaneous curing. In both cases, the cure protocol was the same as for unloaded OC/DDM.

OM of cross sections of two indented nanocomposite specimens (4 wt % CSR loading), made by both methods, are compared in Figure 4. The melt process apparently results in phase segregation >50 μm, while no visible phase segregation occurs using the solution process. Therefore, solution processing was adopted for further studies. Note that no cracks are seen in Figure 4 (compared with Figure 2) around the indentation, suggesting improved fracture toughness.

Fracture Toughness Measurement. Changes in fracture toughness were measured. Figure 5 shows the K_{IC} values vs CSR loading. Each data point is an average of at least five measurements. It is clear that incorporation of CSR improves fracture toughness gradually. At 8 wt % loading, K_{IC} increased from 0.60 ± 0.01 to 0.95 ± 0.05 MPa $m^{1/2}$, an increase of >50%. Up to 2-fold increases in K_{IC} in organic epoxy resins at 5−10 wt % CSR loadings have been reported in the literature.[49−51]

This result suggests that toughening methodologies used for organic epoxies are equally effective in silsesquioxane hybrid matrices. This finding is important because it suggests that general macroscopic composite technologies can be adopted for silsesquioxane thermoset nanocomposites.

However, for this approach to be really valuable, macroscopic modification should not affect the properties optimized by nanoscale modification. Because inclusion of soft, organic-based CSR particles might degrade thermal stability, T_g, and elastic modulus, these properties were examined by TGA, DMA, tensile, and compression tests, as discussed in the following sections.

Thermal Gravimetric Analysis (TGA). Given proof of improvements in fracture toughness, the effects of CSR on other properties were assessed. Thermal stabilities were first tested by TGA. Figure 6 shows the results for three nanocomposites (N_2/5 °C/min). First, both 5% mass loss temperatures and the char yields do decrease with increases in CSR loading. However, the changes are minimal, and the 5% mass loss temperatures remain >400 °C. Furthermore, the main-chain decomposition temperatures of ≈450 °C are also hardly affected. In contrast, the char yields are clearly lower for CSR loaded nanocomposites, but the decrease is smaller than the expected (4 or 8 wt %), suggesting that some CSR remains as char. In general, the incorporation of CSR at up to ≈8 wt % does not degrade thermal stability significantly and only slightly decreases char yields.

Dynamic Mechanical Analysis (DMA). Mechanical stabilities at elevated temperatures were then measured

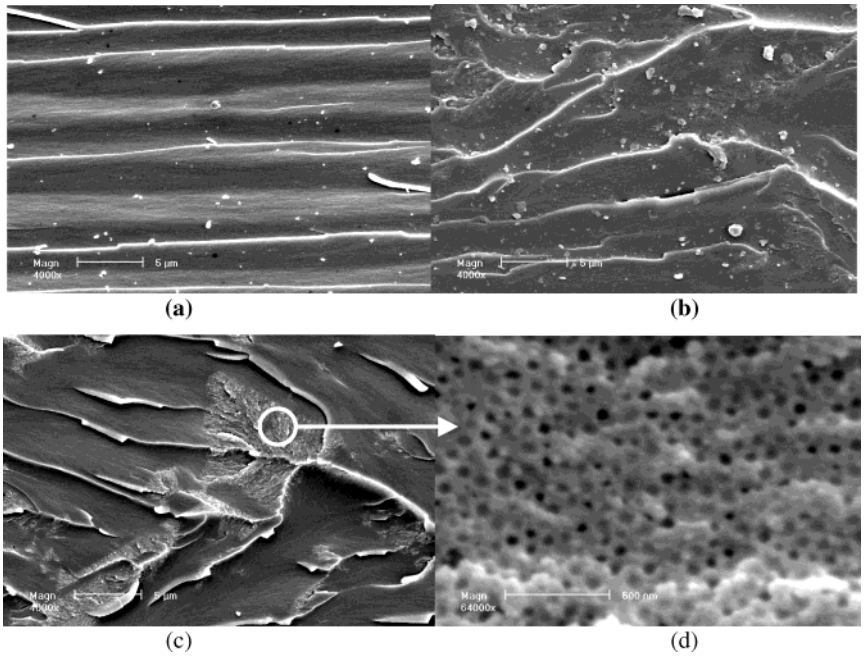

Figure 9. SEMs of OC/DDM/CSR fracture surfaces at (a) 0% CSR, (b) 4% CSR, (c) 8% CSR, and (d) 8% CSR; high resolution. Cracks propagate from left to right.

by DMA. Parts a and b of Figure 7 show the storage modulus and tan δ of the nanocomposites, respectively. The results show that T_g decreases gradually as CSR loadings increase, but only slightly from ~150 to ~130 °C. Although decreases in T_g suggest matrix softening, the effect on fracture toughness is likely minimal considering that the initial K_{IC} was ~0.5 MPa $m^{1/2}$ at a $T_g \sim 110$ °C and because such toughness values are typical of very brittle thermosets and unlikely to become lower. The effects of residual solvent on T_g are also likely small because decreases in char yields are smaller than expected, suggesting that the amounts of residual solvent are negligible. Note that the current cure conditions were selected for a practical cure cycle, and if the cure conditions are changed, T_g can be further improved, e.g., to >160 °C (2 day cure at 200 °C). The rubbery state modulus also decreases slightly as CSR loading increases.

Compression and Tensile Testing. Finally, compression and tensile tests were performed on the new nanocomposites. Nominal stress−strain profiles are shown in Figure 8a,b.

In compression profiles, features typical of materials capable of plastic deformation are found. Initial elastic deformation becomes plastic deformation as the strain passes 0.03 for all three composites. Additionally, the nanocomposites begin to yield at strains of about 0.1 and continue to undergo shear flow until they break. However, these two features are common for all CSR loadings, and distinctive behavior is observed only at failure. These composites fail gracefully at higher CSR loading vs drastic failure at 0 wt % CSR loading, which is consistent with the higher fracture toughness of the CSR loaded composites. Significantly, elastic modulus is preserved completely.

Differences between the materials are more dramatic in tensile tests. In tension, both the ultimate stress and strain increased significantly at the same time as a result of CSR inclusion. As in compression tests, the initial linear elastic deformation changes to nonlinear deformation, but a distinctive yield point is not observed. As in the compression tests, the elastic moduli are not affected by CSR addition.

SEM Studies. The morphology of the nanocomposite fracture surfaces (Figure 8) was studied to identify possible source(s) of toughening.

Distinct surface features are found in each image. These images were taken from behind the crack tips which are on the left sides of the images (cracks propagate from left to right). First, unmodified OC/DDM nanocomposites exhibit fracture patterns that are typical of brittle thermosets. The fracture surface suggests little shear yielding. However, as CSRs are added, the surfaces exhibit more complex patterns. The lines in (b) and (c) are probably due to multiple cracks merging as they grew. The literature indicates that CSR-induced cavitation and shear yielding are typical mechanisms whereby epoxies are toughened.[45−51] Crazing with cavitation and shear yielding is also observed when rubber particles toughen other polymers.[39−44] In this study, CSR cavitation is not observed but CSR pull-out is, at higher resolution (Figure 9d).[45−51] The cavity sizes appear to be ≈100 nm, in accord with CSR sizes determined previously.[3]

The particles in the 8 wt % CSR loaded composite appear to aggregate, forming rubber-rich regions of ~5 μm in a pure OC/DDM matrix. Little evidence for similar segregation is seen in the 4 wt % CSR composites. It appears that the solution process does not fully disperse CSR in the OC/DDM matrix on dilution with extra OC probably because the MEK dissolved or swelled the shell of the CSR, causing the particles to aggregate. Note that phase segregation of rubber-rich regions from pure OC/DDM matrix was not obvious by optical microscopy (OM) because the domain sizes of rubber-rich regions in OM (~5 μm) are relatively small.

It is surprising that the fracture toughness of the nanocomposites increases noticeably despite phase segregation. Usually uniform dispersion is required for optimal toughening. However, it is not clear in this case if phase segregation degrades fracture toughness. In fact, the noticeable increase in fracture toughness

suggests that either phase segregation did not affect the fracture toughness much or the generation of interfaces between the rubber-rich region, and the pure matrix might compensate for the loss in the fracture toughness.

It is thought that phase segregation can be minimized if composites are cured immediately after OC is mixed with extracted CSR without a dilution step. Comparison of these homogeneous composite properties with those of phase-segregated ones will provide a better understanding of phase segregation effects on toughening, and thus in-depth studies will be carried out in the future to investigate this issue.

Discussion

The indentation test is valuable for determining whether a small amount of a specimen of brittle material could be toughenable. In principle, the compression test would reveal the same information but would require much larger specimens. The indentation test showed that toughening was worth pursuing.

The work presented here also suggests that failure mechanisms in nanocomposites can differ considerably from those found in macroscopic composites. However, SEM examination of the fracture surface cannot give clear indications of the actual sequence of deformation events around the crack tip. Further work is required to clarify this issue.

Conclusions

This work provides important guidelines for new strategies that combine molecular level hybridization with macrocomposite strengthening techniques. First, cube nanocomposites are entirely homogeneous and can be used as hybrid matrices for macroscale composites. Furthermore, because the nanocomposite base thermomechanical properties are easily varied by adjusting tether structure, cross-link density, processing condition, etc., various macroscale modification techniques can be used for particular properties. This model study can be extended to include imide nanocomposites[65] and fiber reinforcement to form new hybrid nanocomposites.

Next, little modification is necessary, if any, in applying macroscale modification techniques to hybrid matrices. Toughening effects are also similar to those for organic thermosets. Thus, literature-based modification methods should offer additional methods of toughening.

Last, it appears that macroscale modification of hybrid nanocomposites can have minimal effects on the properties already optimized by nanoscale modification. These results suggest that multiple properties can be improved independently by tailoring the composite structures at nano- and macroscales simultaneously. In this model study, fracture toughness doubles as a result of macroscale modification, while T_g, decomposition temperature, and elastic modulus remain nearly unaffected.

Acknowledgment. This work was supported by AOARD Grant No.-00-4016 to IMRE and by Matsushita Electric Inc. at UM.

References and Notes

(1) Sanchez, C.; Lebeau, B. *MRS Bull.* **2000**, *26*, 377.
(2) Seraji, S.; Wu, Y.; Forbess, M.; Limmer, S. J.; Chou, T.; Cao, G. *Adv. Mater.* **2000**, *12*, 1695.
(3) Rajeshwar, K.; de Tacconi, N. R.; Chenthamarakshan, C. R. *Chem. Mater.* **2001**, *13*, 2765.
(4) Scott, B. J.; Wirnsberger, G.; Stucky, G. D. *Chem. Mater.* **2001**, *13*, 3140.
(5) Corriu, R. *Polyhedron* **1998**, *17*, 925.
(6) Baney, R. H.; Itoh, M.; Sakakibara, A.; Suzuki, T. *Chem. Rev.* **1995**, *95*, 1409.
(7) Kojima, Y.; Usuki, A.; Kawasumi, M.; Okada, A.; Fukushima, Y.; Tarauchi, T.; Kamigaito, O. *J. Mater. Res.* **1993**, *6*, 1185.
(8) Kojima, Y.; Usuki, A.; Kawasumi, M.; Okada, A.; Kurauchi, T.; Kamigaito, O. *J. Appl. Polym. Sci.* **1993**, *49*, 1259.
(9) Vaia, R. A.; Giannelis, E. P. *Chem. Mater.* **2001**, *13*, 3306.
(10) LeBaron, P. C.; Wang, Z.; Pinnavaia, T. J. *Appl. Clay Sci.* **1999**, *15*, 11.
(11) Carrado, K. *Appl. Clay Sci.* **2000**, *17*, 1.
(12) Alexangdre, M.; Dubois, P. *Mater. Sci. Eng.* **2000**, *28*, 1.
(13) Dietsche, F.; Mulhaupt, R. *Polym. Bull. (Berlin)* **1999**, *43*, 395.
(14) Burnside, S. D.; Giannelis, E. P. *Chem. Mater.* **1995**, *7*, 1597.
(15) Gilman, J. W. *Appl. Clay Sci.* **1999**, *15*, 31.
(16) Sanchez, C.; Soler-Illia, G. J. A. A.; Ribot, F.; Lalot, T.; Mayer, C. R.; Cabuil, V. *Chem. Mater.* **2001**, *13*, 3061.
(17) Pyun, J.; Matyjaszewki, K. *Chem. Mater.* **2001**, *13*, 3436.
(18) Schubert, U. *Chem. Mater.* **2001**, *13*, 3487.
(19) Laine, R. M.; Choi, J.; Lee, I. *Adv. Mater.* **2001**, *13*, 800.
(20) Choi, J.; Harcup, J.; Yee, A. F.; Zhu, Q.; Laine, R. M. *J. Am. Chem. Soc.* **2001**, *123*, 11420.
(21) Choi, J.; Lee, I.; Yee, A. F.; Laine, R. M. *Chem. Mater.* **2003**, *15*, 5666.
(22) Choi, J.; Kim, S.; Tamaki, R.; Laine, R. M. *Macromolecules* **2003**, *37*, 99.
(23) Zhang, C.; Babonneau, F.; Bonhomme, C.; Laine, R. M.; Soles, C. L.; Hristov, H. A.; Yee, A. F. *J. Am. Chem. Soc.* **1998**, *120*, 8380.
(24) Zhang, C.; Laine, R. M. *J. Am. Chem. Soc.* **2000**, *122*, 6979.
(25) Tamaki, R.; Tanaka, Y.; Asuncion, M. Z.; Choi, J.; Laine, R. M. *J. Am. Chem. Soc.* **2001**, *123*, 12416.
(26) Kang, S.; Hong, S.; Choe, C.; Park, M.; Rim, S.; Kim, J. *Polymer* **2001**, *42*, 879.
(27) Koh, S.-W.; Kim, J.-K.; Mai, Y.-W. *Polymer* **1993**, *34*, 3446.
(28) Nakamura, Y.; Yamaguchi, M. *Polymer* **1992**, *33*, 3415.
(29) Kornmann, X.; Lindberg, H.; Berglund, L. A. *Polymer* **2001**, *42*, 4493.
(30) Lee, A.; Lichtenhan, J. D. *J. Appl. Polym. Sci.* **1999**, *73*, 1993.
(31) Wang, Z.; Pinnavaia, T. J. *Chem. Mater.* **1998**, *10*, 1820.
(32) Lan, T.; Pannavaia, T. J. *Chem. Mater.* **1994**, *6*, 2216.
(33) Messersmith, P. B.; Giannelis, E. P. *Chem. Mater.* **1994**, *6*, 1719.
(34) Sue, H.-J.; Pickelman, D. M. In *Elastomer Technology Handbook*; Cheremisinoff, N. P., Ed.; CRC Press: Boca Raton, FL, 1993.
(35) Sue, H.-J. *J. Mater. Sci.* **1992**, *27*, 3098.
(36) Choi, J.; Weaver, J.; Sue, H.-J.; Laine, R. M., unpublished work.
(37) Plummer, C. J.; Beguelin, P.; Kausch, H.-H. *Colloids Surf.* **1999**, *153*, 551.
(38) Cruz-ramos, C. A. In *Polymer Blends;* Paul, D. R., Bucknall, C. B., Eds.; John Wiley & Sons: New York, 1999; Vol. 2, p 137.
(39) Wong, S.-C.; Mai, Y.-W. *Polymer* **2000**, *41*, 5471.
(40) Crawford, E.; Lesser, A. J. *Polymer* **2000**, *41*, 5865.
(41) Luzinov, I.; Pagnoulle, C.; Jerome, R. *Polymer* **2000**, *41*, 7099.
(42) Wal, A.; Gaymans, R. J. *Polymer* **1999**, *40*, 6067.
(43) Wei, G.-X.; Sue, H.-J. *Polym. Eng. Sci.* **2000**, *40*, 1979.
(44) Yu, Z.; Ou, Y.; Qi, Z.; Hu, G. *J. Polym. Sci., Part B: Polym. Phys.* **1998**, *36*, 1987.
(45) Bucknall, C. B. In *Polymer Blends;* Paul, D. R., Bucknall, C. B., Eds.; John Wiley & Sons: New York, 1999; Vol. 2, p 83.
(46) Kinloch, A. J. In *Rubber-Toughened Plastics*; Keith, C., Ed.; American Chemical Society: Washington, DC, 1989; p 67.
(47) Takahashi, T.; Nakajima, N.; Saito, N. In *Rubber-Toughened Plastics*; Riew, C. K., Ed.; American Chemical Society: Washington, DC, 1989; p 243.
(48) Oh, B.; Kim, H.; Ma, P. In *Toughened Plastics II: Novel Approaches in Science and Engineering*; Riew, C. K., Kinloch, A. J., Eds.; American Chemical Society: Washington, DC, 1996; p 111.
(49) Sue, H.-J.; Puckett, P. M.; Bertram, J. L.; Walker, L. L.; Garcia-Meitin, E. I. *J. Polym. Sci., Part B: Polym. Phys.* **1999**, *37*, 2137.
(50) Ashida, T.; Katoh, A.; Handa, K.; Ochi, M. *J. Appl. Polym. Sci.* **1999**, *74*, 2955.
(51) Xiao, K.; Ye, L. *Polym. Eng. Sci.* **2000**, *40*, 70.

(52) Wu, H.; Xu, J.; Liu, Y.; Heiden, P. *J. Appl. Polym. Sci.* **1999**, *72*, 151.
(53) Yee, A. F.; Pearson, R. A. *J. Mater. Sci.* **1986**, *21*, 2462.
(54) Pearson, R. A.; Yee, A. F. *J. Mater. Sci.* **1986**, *21*, 2475.
(55) Lu, J.; Wei, G.-X.; Sue, H.-J. Sue; Chu, J. *J. Appl. Polym. Sci.* **2000**, *76*, 311.
(56) Lee, J.; Yee, A. F. *Polymer* **2001**, *42*, 577.
(57) Rice, Jr.; Ben-Zion, Y.; Kim, K. *J. Mech. Phys. Solids* **1994**, *42*, 813.
(58) Groleau, M. R.; Shi, Y.-B.; Yee. A. F.; Bertram, J. L.; Sue, H.-S.; Yang, P. C. *Composites Sci. Technol.* **1996**, *56*, 1223.
(59) Tanaka, Y. In *Epoxy Resins, Chemistry and Technology*; May, C. A., Ed.; Marcel Dekker: New York, 198
(60) 8; p 9.
(61) Goodman, S. H. In *Handbook of Thermoset Plastics*; Goodman, S. H., Ed.; Noyes Publ.: Westwood, NJ, 1998; p 193.
(62) Smith, G.; May, C. A. In *Epoxy Resins*; Gould, R. F., Ed.; American Chemical Society: Washington, DC, 1970; p 140.
(63) Bucknall, C. B. *Toughened Plastics*; Applied Science Publishers Ltd.: Essex, UK, 1977; p 182.
(64) Haung, Y.; Kinloch, A. *J. Mater. Sci.* **1992**, *27*, 2763.
(65) Cardwell, B. J. Toughening of polymer blends through thermoplastic additions. Ph.D. Dissertation, University of Michigan, Ann Arbor, MI, Dec 1994.
(66) Choi, J.; Kim, S.; Tamaki, R.; Laine, R. M. *Chem. Mater.* **2003**, *15*, 3365.

MA0303723